# THREE DIMENSIONAL EFFECTS OF LIQUID WATER FLOODING IN THE CATHODE OF A PEM FUEL CELL

by

Dilip Natarajan and Trung Van Nguyen*
Department of Chemical and Petroleum Engineering
University of Kansas
Lawrence, KS 66045, USA

Submitted as
A Research Paper

To

Dr. C. K. Dyer
The Journal of Power Sources
16 Seven Oaks Circle
Madison, New Jersey 07940-1314
USA

1st submission: October 24, 2002

**Final Version**

Key words: Fuel cell, conventional gas distributor, interdigitated gas distributor, cathode, electrode, mathematical model, pseudo three dimensional

* Author to whom correspondence should be addressed

## ABSTRACT

A two-dimensional model available in the literature for conventional gas distributors was expanded to account for the dimension along the length of the channel. The channel was discretized into control volumes in series that were treated as well mixed. An iterative solution procedure was incorporated in each control volume to determine the average current density and the corresponding oxygen consumption and water generation rates. Down stream channel concentrations were calculated based on stoichiometric flow rates and the solution obtained from the preceding control volumes. Comparison of the model results with experimental data and the existing two-dimensional model showed that accounting for the oxygen concentration variations along the channel and its effect on the current density is critical for accurately predicting the cathode performance. Variations in the current density along the channel were strongly influenced by the changes in oxygen concentration caused by consumption due to reaction and dilution caused by water evaporation. Operating parameters that facilitated better water removal by evaporation like higher temperature and stoichiometric flow rates and lower inlet stream humidity resulted in higher net current. Operating conditions that resulted in minimal loss in oxygen concentrations resulted in a more uniform current density distribution along the channel.

## Introduction

Over the last decade, Proton Exchange Membrane (PEM) fuel cells have emerged as viable energy conversion devices for terrestrial applications such as power generation and transportation. Researchers all over the world are focusing on optimizing this system to be cost competitive with energy conversion devices currently available. It is a well known fact that the cathode of the PEM fuel cell is the performance limiting component due to the slower oxygen reduction kinetics and mass transport limitations imposed by the liquid water generated by the electrochemical reaction and electro-osmotic drag. The liquid water can hinder transport of the reactant species by blocking the pores in the porous gas diffusion layer and by covering up active sites in the catalyst layer. Another performance limiting component can be the ion conducting polymeric membrane (Nafion). The conductivity of this membrane, which consists of a fluorocarbon polymer backbone with chemically bonded sulfonic acid groups as side chains, is a very strong function of its water content. Severe dehydration of the membrane can result in significantly high ohmic losses in performance. Thus the optimization of PEM fuel cells is basically a water management problem.

The inherent difficulties in conducting experiments to determine the actual distribution of water in the membrane, catalyst and diffusion layers, and its effect on reactant species in an operating fuel cell have prompted researchers to develop representative mathematical models to gain qualitative insights into the dynamics of liquid water and its effect on the fuel cell performance. Pioneering work in fuel cell modeling were usually one dimensional, representing the direction normal to the reactive catalyst surface, and accounted only for gaseous phase to avoid the complexities involved in multi-dimensional modeling of multi-phase flow in porous media[1,2,3&4]. Though these models provide excellent qualitative information, the model

predictions are not representative of 'real life' situations and cannot correctly account for the presence of liquid water in the gas diffusion and catalyst layers and its influence on gas transport. Moreover, these one-dimensional models cannot correctly predict and compare the effects of different flow distribution strategies employed by the use of different types of gas distributors.

In the past, fuel cell researchers used conventional or serpentine gas distributors where convective gas flow is predominantly restricted to the flow channels while the transport of gaseous species in the diffusion layers is mainly by diffusive mechanism. Moreover, liquid water dynamics in the diffusion layers is dominated by capillary phenomenon. Recently our research group came up with an interdigitated gas distributor design that forces convective gas flow through the diffusion layers[5]. In this type of a flow field, both convective and diffusive mechanisms are significant mass transport means for the gas phase, while liquid transport is affected by both capillary forces and gas flow induced drag forces.

Over the past few years researchers have been looking into multi dimensional, multi phase models to accurately predict the performance of PEM fuel cells employing both conventional and interdigitated flow distributors. Nguyen et al [6] developed a heat and water management model that included the dimensions normal to the reactive interface and along the channel. However, they ignored the diffusion layer and accounted only for the membrane with a catalyst interface on the anode and cathode sides. Fuller et al [7] also developed a similar model around the same time. Both these models concentrated on the temperature and water vapor profiles along the channel and the membrane water content profile under different operating conditions. West et al [8] developed one of the first two-dimensional models for conventional gas distributors where they looked at the dimension parallel to the reactive surface (other than the dimension along the channel) to analyze the effect of rib spacing. Their modeled domain included the gas diffusion layer and the membrane. Their model accounts for liquid water only in

the membrane and not in the diffusion layer and does not account for the dimension along the length of the channel. Gurau et al [9] developed a two-dimensional model for the entire fuel cell sandwich employing conventional gas distributors that accounted for the diffusion layer. The dimension normal to the reactive surface and the dimension along the length of the channel were considered. However, they accounted for liquid water only in the membrane and the catalyst layers and not in the porous gas diffusion layers. Singh et al [10] came up with a two dimensional model for the fuel cell sandwich similar to that of Gurau et al's work. While, Gurau et al employed an iterative procedure to calculate the concentration of the reactant and product species along the length of the channel, Singh et al assumed a linear variation of species concentration along the channel.

Dutta et al [11] developed a complete three-dimensional model to include the dimension parallel to the reactive surface, i.e. the electrode width, to account for the electrode regions hidden from the gas channel. Their modeled domain covered the entire fuel cell sandwich employing conventional gas distributors on both the anode and the cathode sides. However, they fail to account for liquid water in the gas diffusion layers. Shimpalee et al [12] extended this work to include liquid water. They treat the liquid water as a component of the gas mixture, transported by convection by gas pressure and density gradients. Furthermore, the effect of liquid water and its distribution in the porous gas diffusion layer on the gas transport and the electrochemical reactions were not accounted for either by Gurau et al, or Shimpalee et al. Natarajan et al[13] recently published a two dimensional model that considered the dimension normal to the reactive surface and the electrode width. In this work, gas transport was modeled by Stefan-Maxwell multi-component diffusion equations, while Darcy's law was adapted to model liquid water transport in unsaturated porous gas diffusion layers. Here the effect of liquid water accumulation in the diffusion layer was accounted for in terms of gas transport restrictions

and reactive surface coverage. Um et al[14] developed a transient multidimensional model that simultaneously accounts for electrochemical kinetics, current distribution, hydrodynamics and multi-component transport to study hydrogen dilution effects. Similar to Shimpalee et al's work, a multiphase homogeneous mixture model approach was used by the authors that assume the liquid water phase to be a part of the gas mixture.

A few researchers have also directed their modeling efforts to address fuel cells employing interdigitated gas distributors. Yi et al [15] came up with one of the first modeling attempts on PEM cathode using interdigitated flow fields. This was a single-phase model that did not consider the liquid water phase. Yi et al [16] later included liquid water in their two dimensional model to more accurately describe the transport phenomena in the fuel cell cathode. Yi et al's later work used mass based conservation equations, which are quite inconvenient for current density and interfacial mass transfer calculations. Moreover, the liquid water flow induced by capillary forces and gas flow induced drag was addressed by semi-heuristic equations. This model was later modified by He et al [17] to a molar basis with a more robust and realistic interfacial mass transfer equation for water vaporization and condensation. The equation of motion for liquid water was also modified to account for water movement by both capillary and gas shear induced forces. Wang et al [18] also came up with a similar two-dimensional multi phase model based on a multiphase homogeneous mixture model as in Shimpalee et al's work, to describe the transport processes involved in an interdigitated cathode.

As seen from the above literature review, modeling efforts have been focused towards eventually developing a comprehensive model that covers the entire fuel cell sandwich including the anode, cathode and the membrane components. Though such a model that accurately describes the phenomena involved will be tremendously helpful, one needs a viable experimental tool such as a reference electrode that separates the cell voltage loss into its individual

components to validate the model with experimental results. Moreover, when proper anode humidification and heat management schemes are employed in a fuel cell, liquid water flooding in the cathode diffusion layer becomes the crucial limiting factor justifying attempts to develop representative models for the cathode chamber alone that helps to develop an idea of desirable operating parameters. Moreover, there is a significant advantage in accounting for the 3rd dimension along the channel as compared to a pure 2-D model in terms of validation with experimental data, which will be brought out in the latter sections.

In this paper a pseudo three- dimensional model is developed by extending the two-dimensional isothermal model developed by Natarajan et al [13] for cathodes using conventional gas distributor, to include the third dimension along the channel. The model was used to obtain qualitative insights into the distribution of liquid water in the diffusion layer and its effect on the distribution of the gas phase reactant species. Operating parameters like temperature, stoichiometric flow rate and inlet gas stream humidity were evaluated. Furthermore, the predictions of 2-D and 3-D models were evaluated with respect to experimental data.

## Model Development

Figure 1 show the schematic of the cross section of the modeled domain at the entrance of the channels for the conventional distributor. The modeled domain consists of a region of half the width of the channel and shoulder and the gas diffusion layer and a reactive gas-diffuser-membrane interface above this region. The other half of the shoulder and channel can be considered as a mirror image and need not be explicitly solved for. Regarding important assumptions and other model considerations, the reader is referred to the authors' previous publications [13] for the sake of brevity.

Governing Equations

A brief summary of the model equations used in the 2-D model developed in a previous publication is provided here along with a detailed description of the development of the pseudo 3-D model based on them. Table 1 provides a brief summary of the governing equations used by Natarajan et al [13]. Further details on the governing equations can be found elsewhere[13]. Table 2 provides the relevant parameters pertaining to the 3-D models that are different from the previous 2-D simulations. In the conventional flow field model, the Stefan-Maxwell [19] multi-component diffusion equations were used to account for the diffusive flux in the gas phase, while the Richard's equation [20] adapted from hydrology literature for unsaturated flow in porous media was used to describe liquid water flux within the diffusion layer. These flux terms were substituted into general continuity equations as applied to porous media to provide the governing equations for oxygen and water vapor mole fractions and liquid water saturation. The governing equations of the gas phase and liquid water are coupled through the effective diffusivity term that accounts for the presence of liquid water in the gas pores. The water vapor and liquid water continuity equations are also coupled through an interfacial mass transfer rate.

In the case of the 3-D model for conventional gas distributors, the length of the channel is divided into a series of control volumes that has a gas-diffuser and a channel volume associated with it. The boundary condition at the reactive interface and over the shoulder is same as in the 2-D model. Moreover within the diffusion layer, for a given control volume, it is assumed that there is no change in the magnitude of the solved-for variables in the direction along the channel length. This implies that all the gradients at the boundaries of the control volumes are forced to zero. However, the channel volume in each of these control volumes is assumed to be perfectly mixed. Figure 2 is a schematic representation of the solution procedure. For the first volume element, the oxygen and water vapor mole fractions and liquid water saturation boundary

conditions at the channel-diffusion layer interface are set to the inlet conditions and the 2-D model is solved to provide a given rate of oxygen consumption and water vapor and liquid water generation. Based on these fluxes, and a given stoichiometric flow rate of air, the boundary conditions in terms of mole fractions and saturation are calculated and the 2-D model is solved again. This iterative process is repeated till the change in the boundary conditions is negligible. Having thus obtained a solution for the first volume element, the initial guess of boundary conditions for the channel-diffusion layer interface for the subsequent volume element is calculated again based on the first volume element's flux solution and stoichiometric flow rate and the above mentioned iterative process is repeated. Moreover, liquid water generated by reaction and electro-osmotic drag is allowed to completely evaporate till the gas stream is saturated. Once the gas stream is saturated the water vapor boundary conditions for subsequent volume elements are forced to the saturation pressure, while liquid water saturation at these boundaries is forced to 0.1. The rationale behind this boundary condition for liquid water at the channel – diffusion layer interface is explained in detail in the following sections.

A brief analysis of the liquid and gas phase transport processes involved in the cathode of a PEM fuel cell using conventional gas distributors is necessary at this juncture to justify the approach used in this model. Figure 3 is another schematic view of the cathode chamber of the fuel cell along the length of the channel. Oxygen that is supplied at the inlet of the channel is transported convectively along the length of the channel while diffusion is the sole mechanism of transport through the diffusion layer in the direction towards the reactive catalyst layer. The liquid water generated by the electrochemical reaction is removed from the catalyst layer by two mechanisms namely, evaporation and diffusion of water vapor and liquid water transport. The water vapor transport process is similar to the oxygen species, i.e. diffusion away from the reaction zone through the diffusion layer and convection in the gas channel. In a typical fuel cell

cathode, the dimension along the z-direction (in the order of centimeters) is much greater than that of the y-direction normal to the reactive layer or interface (in the order of a few hundred microns) and x-direction, parallel to the reactive plane (in the order of a few millimeters). It is based on this aspect ratio that the authors assumed that diffusion within the diffusion layer in the z-direction is insignificant especially when transport in that direction is dominated in the channel by a much faster convective process. This assumption has been implemented in the model by assuming no gas transport in the z direction within the diffusion layer between the control volumes along the channel. However, the model takes into account the change in the gas composition in the channel down its length due to consumption of oxygen and water evaporation in the preceding control volumes.

Liquid water is transported solely by a capillary mechanism within the diffusion layer. Once liquid water reaches the channel – diffuser interface it is transported along the length of the channel by the drag force exerted on the liquid due to the convective flow of gas in the channel. Since evaporation and water vapor transport are relatively much faster than liquid water transport, one can expect to observe liquid water in the channel only after the gas phase has been completely saturated with water vapor. Up to this point the water that ‘wicks’ out of the diffusion layer completely evaporates in the channel. Beyond this point of complete gas saturation with water vapor, liquid water appears in the channel and the rate of its transport and distribution in the channel depends on the gas velocity and the wetability of the channel material which is usually graphite. This rate of water movement is assumed to be faster than the capillary phenomenon within the diffusion layer. Hence the same approach as that of gas phase is implemented for liquid water where the movement of water in the z-direction within the diffusion layer is assumed to be insignificant as compared to the movement of water due to gas drag in the channel. However, beyond the point of water vapor saturation of the gas stream, the

liquid water that is present in the channel can reduce the rate of wicking from the diffusion layer down stream. In other words, once liquid water is present in the channel, the channel – diffusion layer interface is no longer dry (i.e. saturation at this interface is no longer 0) and this reduces the water saturation gradient in the diffusion layer down stream thereby reducing the rate of water transport by capillary action. The model does not account for momentum effects in the channel and hence does not explicitly solve for gas phase species concentration and liquid water amounts. To qualitatively capture the onset of liquid water presence in the channel once the gas stream is saturated, the water vapor boundary conditions for subsequent volume elements are forced to the saturation pressure, while liquid water saturation at these boundaries is forced to 0.1. This non-zero value can be rationalized by the fact that one can never achieve zero saturation in porous media when the gas is saturated, for there always exists an irreducible water saturation, which can be removed only by evaporation and not by any kind of transport mechanism [21]. The authors do recognize that this value of 0.1 for liquid water saturation is arbitrary. However, it does provide qualitative information as to how far from the inlet that one can expect to see the appearance of liquid water in the channel.

It is a well established fact that gas phase transport is much faster than liquid water dynamics and it is the slower water removal mechanism that is the performance limiting criterion of the cathode of PEM fuel cells. Other than removal by evaporation, there exists two distinct steps in the liquid water removal mechanism as explained above. Liquid generated at the catalyst layer has to 'wick' through the diffusion layer to the channel – diffusion layer interface from where it is transported down the channel and out of the cathode chamber by gas flow in the case of a conventional gas distributors. Of these two steps, our hypothesis is that the capillary wicking process within the diffusion layer is the limiting step. The well documented poor performance of cathodes with conventional distributors in literature [22] even at very high stoichiometric air flow

rates and high temperatures that avoid liquid water presence in the cathode layer is ample proof for this hypothesis. In other words, if the diffusion layer near the reaction interface (or catalyst layer) and above the shoulders is not severely flooded, the cathode reactive area can support much higher current based on unrestricted gas transport. Thus even under operating conditions when liquid water presence in the channel is avoided completely, the diffusion layer is usually flooded to restrict mass transport and hence reduce oxygen reduction reaction rates. The better performances of cathodes with interdigitated [22] or serpentine flow fields that cause the gas to flow through the diffusion layer and hence remove water from the diffusion layer by a faster convective process are also supporting evidence for our above mentioned hypothesis. The authors however recognize the fact that once liquid water is present in the channel the rate of water wicking from the diffusion layer beyond this point can be severely reduced leading to increased flooding and lower current densities down stream. The authors also clearly recognize that by arbitrarily forcing the boundary condition to 0.1 beyond this point the model cannot truly capture the severity of flooding beyond this point and the model predictions are quite qualitative once liquid water is present in the channel.

Moreover, it is our contention that accounting for the 3rd dimension along the length of the channel even with its inherent assumptions is quite crucial to reasonably predict the magnitude of the capillary water removal rate from the diffusion layer that is the crucial limiting step in the cathode as shown in the following section.

## Results and Discussion

Comparison with Experimental Data

In Natarajan et al's [13] work, experimental data was generated with a specially fabricated Membrane Electrode Assembly (MEA) that included a built-in reference electrode. This reference electrode facilitated the measurement of individual half-cell potentials that were suitable for comparison with model results. The relevant experimental conditions are available in Reference 13. A stoichiometric air flow rate of 1.2 A/cm$^2$ was used in the experiment. The authors adjusted the exchange current density and the rate of liquid water removal from the diffusion layer to fit the model results to the experimental data. Figure 4 provides the experimental results, the 3-D model fit from this work and the predictions of the 3-D model applying the parameters used in Natarajan et al's 2-D simulations. It is clear from Figure 4 that when 2-D model parameters were used in the 3-D model and simulated at a stoichiometric flow rate of 1.2 A/cm$^2$, the model under-predicted the cathode performance. Natarajan et al [12] assumed that a stoichiometric flow rate of 1.2 A/cm$^2$ was high enough to neglect the drop in oxygen concentration along the length of the channel for the entire range of current densities. However, at a flow rate of 1.2 A/cm$^2$, there is a significant drop in the oxygen concentration even at moderate operating overpotentials, which results in lower current densities along the length of the channel as shown in the latter sections. By not accounting for the dimension along the length of the channel, Natarajan et al's 2-D work did not take into consideration the drop in the oxygen concentration and its effect of lower current densities down the channel. Thus the water removal rate in the 2-D model was under-predicted to fit the model results to experimental data. Hence the liquid water removal rate was increased in the 3-D model simulations to fit the experimental data. A comparison between this work and the authors' previous work shows the importance of

accounting for all the dimensions when modeling a conventional flow field. On the contrary, it is interesting to note that when modeling interdigitated flow fields, if one assumes negligible pressure drop along the length of the channel as compared to the drop across the diffusion layer over the shoulder, which is quite a valid assumption, one can ignore the dimension along the channel for modeling purposes.

It needs to be pointed out here that though the pseudo 3-D model provides a more realistic case for comparison with experimental data as compared to a 2-D model, the results of the 3-D model might still under predict the capillary water removal rate. As explained above, by arbitrarily setting the boundary condition at the channel – diffusion layer interface to 0.1 after the point of complete vapor saturation of the gas stream, this model does not quantitatively capture the severity of flooding beyond this point. It is our view that in the regions beyond the point of complete saturation of the gas stream with water vapor, the severity of diffusion layer flooding increases significantly leading to a more non-uniform current density distribution than the prediction by this model. If this were the case, then to achieve the same average current density (measured experimentally) over the entire length of the channel, the local current densities in the region before the point of complete vapor saturation of gas stream will have to be much higher, which in turn can be achieved only if there is a greater rate of liquid water removal from the diffusion layer and hence lesser extent of flooding.

These new set of parameters were used as the base case to evaluate various operating conditions like stoichiometric flow rates, inlet stream humidity and temperature. Table 2 provides the new parameters that are different from Natarajan et al's work and those that are relevant to a three-dimensional model domain. Other information regarding base case parameters can be found elsewhere[13]. The case studies conducted in this work are presented in the form of polarization curves. Current density distribution along the electrode width and water distribution

in the diffusion layer is provided for the base case. Figure 5a and 5b provides the distribution of liquid water in the gas diffusion layer in a conventional flow field configuration at the entrance and exit. As seen clearly from these figures, liquid water accumulates significantly over the shoulder and all over the width of the electrode except near the channel-diffusion layer interface. This accumulated water imposes severe mass transport limitations by blocking the gas pores and by covering up the reactive surface area. Figure 6 is a plot of the local current densities along the width of the electrode and the length of the channel for the conventional gas distributor. The reactive area over the shoulder is severely flooded leading to negligible contribution from this region to the net current. Moreover, a drop in the current is observed along the length of the channel that is attributed to the drop in oxygen concentration.

Effect of Stoichiometric Flow Rate

Figure 7 provides the polarization curves for the cathode at different stoichiometric flow rates. Figure 8 provides a plot of the average current density over each control volume along the length of the gas channel. In a conventional gas distributor, as one increases the air flow rate, the drop in the oxygen concentration along the length of the channel decreases leading to higher current densities further down the channel. At low stoichiometric flow rates like 0.6 $A/cm^2$, one sees a distinct two-slope region in the current density profiles. Near the entrance of the channel, the gas is still unsaturated in terms of water vapor and the current density drops steeply due to the dilution of oxygen in the air stream, as a result of consumption of oxygen and evaporation of water in the preceding control volumes leading to lower oxygen concentration available for subsequent control volumes down the length of the channel. Eventually, enough water is generated and evaporated to completely saturate the gas stream with water vapor. At this point

one starts observing liquid water in the channel. Beyond this point of saturation, the slope of the current density profile, which only represents the consumption rate of oxygen by the electrochemical reaction, is gentler compared to the slope of the current density profile up to the point of saturation. Here again, the slope after the point of saturation would be a lot steeper if the presence of liquid water in the channel and its negative effect on water removal from the diffusion layer were more quantitatively accounted for.

The slopes of both regions appear to become steeper with decreasing stoichiometric flow rates. From the relative magnitudes of the slopes before and after saturation, it is evident that the dilution effect is the dominant cause of non uniform oxygen and consequently current density distribution along the channel. This strongly suggests that the liquid water in the diffusion layer and its mass transfer hindering effects dominates the performance of the cathode. This conclusion is further augmented in the following section on the effect of inlet stream humidity.

As the stoichiometric flow rate is increased, the evaporation capacity is increased and the point of saturation is pushed further down the channel. Eventually, if the flow rate is high enough, the gas never reaches saturation resulting in a single slope profile. Moreover, as the ratio of the flow rate to the consumption rate, the latter being dominated by liquid water accumulation in the diffusion layer, is increased, one observes a gentler slope in the current distribution profile. Thus at higher stoichiometric flow rates, the oxygen concentration along the channel is more uniform and close to the inlet values resulting in better performance as seen in the polarization curves in Figure 7. It should also be noted that even at the base case stoichiometric flow rate of 1.2 $A/cm^2$ the current density drops by about 40% along the length of the channel and can be attributed to the drop in oxygen concentration. Two-dimensional models that do not account for the dimension along the length of the channel cannot account for this oxygen depletion effect. The cathode performance at infinite stoichiometric flow rate is also provided in Figures 7 and 8

where there is no change in the air stream composition along the length of the channel. The 2-D model predictions are valid only under such operating conditions where changes in the air stream composition along the channel can be ignored. It should be noted that the predictions of this model (same as that of 2-D model) at infinite stoichiometric flow rate are well within the range of the best performance data obtained with conventional flow fields commonly encountered in literature. This suggests that even when the channel is completely devoid of water, the diffusion layer is still flooded due to slow water removal by capillary action leading to poor overall performance. If this were not the case, unrestricted gas diffusivities should be able to sustain more than ten times the current densities observed in experiments.

Effect of Inlet Stream Humidity

Figure 9 provides the polarization curves for the air cathode at various inlet stream relative humidity, while Figure 10 provides the current density distribution along the channel. The polarization curves in Figure 9 suggest that the performance of the cathode decreases with increasing inlet stream humidity. On analyzing Figure 10, it is seen that at 100% inlet stream humidity, the current density distribution along the length of the channel is almost uniform and any drop in oxygen concentration due to consumption is quite negligible. As one drops the inlet stream humidity, the performance of the cathode increases near the inlet up to a certain point down the channel where it reaches complete saturation. This point of saturation is pushed further down the channel as the inlet stream gets drier. This increase is due to higher oxygen concentration available in unsaturated air stream. This observation also suggests that the non-uniformity in the oxygen concentration along the channel and hence the uneven current density distribution is mainly due to the dilution effect of the inlet gas stream by evaporation. It should

be noted that if the diffusion layer properties were changed to enhance liquid water removal, the consumption of oxygen could become significant in affecting the current density profile.

At first glance the results under this case study seem to contradict experimental data that shows better cell performance with increasing cathode stream humidity. However to address this issue, it should be noted that this model does not address the membrane dehydration and its effect on the current density profile. Hence the discrepancy between the model and experimental results is probably due to the fact that the experiments were conducted under conditions were the anode was not properly humidified and hence any increase in the cathode stream humidity improved the hydration levels of the membrane leading to improved performance with increasing cathode feed stream humidity. The model will provide results more representative of experimental data if the membrane is included in the modeled domain to account for the effects of dehydration.

Effect of Temperature

The polarization curves at different operating temperatures are provided in Figure 11. The current density distribution along the length of the channel for the conventional case is provided in Figure 12. As expected, the performance of the cathode is enhanced over the entire overpotential range. As the temperature is increased, the exchange current density and the water removal rate by evaporation are enhanced. It should be noted that the dependence of capillary phenomenon on temperature is not accounted for. The higher exchange current density at higher temperature results in higher current density along the entire length of the channel in the conventional flow field as seen in Figure 12. However, at higher temperatures, one sees a more non-uniform current distribution. This is because increasing temperature result in higher saturation pressure for water vapor which in turn increases the evaporation capacity of the gas stream. At lower temperature, the dilution of oxygen in the air stream due to evaporation is less

prominent. At low temperatures and stoichiometric flow rates, one can expect that the consumption of oxygen is the dominant reason for reducing oxygen concentrations along the length of the channel rather than the dilution of the stream by evaporation.

## Conclusions

A three-dimensional model was developed for the cathode of a PEM fuel cell using a conventional gas distributor. The model results were validated against experimental data and the predictions were compared to existing two-dimensional models. Three-dimensional models that included the dimension along the length of the channel properly accounted for the drop in oxygen concentration in the channel due to consumption and dilution and its effect on the performance of the cathode. Two-dimensional models currently available in literature cannot account for this phenomenon and tends to under-predict the liquid water removal rate when fitted against experimental data. Higher stoichiometric flow rates resulted in more uniform current density distribution along the channel resulting in better cathode performance. The model was also able to predict the distance from the inlet where the gas stream becomes completely saturated with water vapor resulting in the appearance of liquid water in the channel at various operating conditions. The performance of the cathode was found to decrease with increasing inlet stream humidity. Higher temperatures resulted in non uniform current density distribution along the length of the channel and higher average performance of the entire cathode.

Based on the predictions of this model and the authors' previous publications, it can be concluded that the liquid water transport mechanism is the slowest and most dominant in influencing the performance of the cathode. The results from the 3-D model suggest that the current density distribution along the channel is strongly dependent on the oxygen concentration

profile along the channel. The oxygen profile is influenced by consumption due to the electrochemical reaction and dilution due to water evaporation. The relative contribution of these two phenomena is greatly influenced by operating conditions like stoichiometric flow rate, inlet stream humidity and operating temperature.

## Acknowledgment

This work was supported by the National Science Foundation under grant no. CTS-9910923.

## List of Symbols

A empirical constant

$a_0$ available reaction area, $cm^2/ cm^2$

B empirical constant

C empirical constant

$C_T$ molar density, $moles/cm^3$

D empirical constant (cm)

$D_{ij}^e$ effective binary diffusion coefficient $cm^2/s$

F Faraday's constant, 96487 C/equivalent

$F_i$ molar flow rate of species i, moles/s

$F_T$ total molar flow rate, moles/s

g acceleration due to gravity, $cm/s^2$

I current density, $A/cm^2$

$I_0$ exchange current density, $A/cm^2$

$I_{2\text{-}D}$ current density solution from 2-D model ($A/cm^2$)

K permeability, $cm^2$

$k_c$ condensation constant, $s^{-1}$

$k_e$ evaporation constant, cm/atm-s

$K_{l,abs}$ absolute permeability of liquid water, $cm^2$

$k_{l,rel}$ relative permeability of liquid water, $cm^2$

$m_w$ molecular weight of liquid water, gm/mole

$N_i$ molar flux of species i, moles/$cm^2$-s

P pressure, atm

$P_{H2O}^{sat}$ saturation pressure for water vapor, atm

$P_{ref}$ reference pressure, atm

$q_w$ liquid water flux, cm/s

$R_x$ oxygen consumption rate due to reaction, moles/$cm^2$.s

R universal gas constant, 82.06 $cm^3$atm/mole or 8.314 J/mole-K

$R_i$ homogenous reaction rate for species i, moles/$cm^3$-s

s water saturation (liquid volume / dry void volume)

T temperature, °C

*t* time, s

$t_x$ electrode width (cm)

x x dimension (parallel to electrode)

$x_i$ mole fraction of species i

$x_i^{new}$ dummy mole fraction variable used in iterative calculations

y y dimension (normal to electrode)

y y dimension (parallel to electrode)

z z dimension (along the channel)

$\Delta z$ length of control volume (cm)

Greek letters

| | |
|---|---|
| $\alpha$ | net water transfer coefficient per proton |
| $\alpha_c$ | cathodic transfer coefficient |
| $\varepsilon_0$ | porosity of electrode |
| $\eta$ | overpotential for oxygen reduction reaction, V |
| $\mu$ | viscosity of liquid water, gm/cm-s |
| $\rho_w$ | density of liquid water, gm/cm$^3$ |
| $\psi$ | capillary head, cm |

Subscripts and superscripts

| | |
|---|---|
| e | effective |
| $H_2O$ | water vapor |
| i | species i |
| in | channel inlet |
| j | species j |
| $N_2$ | nitrogen |
| $O_2$ | oxygen |
| w | liquid water |

## References


1. T. E. Springer, M. S. Wilson and S. Gottesfeld, *J. Electrochem. Soc.*, **140**, 3513 (1993).
2. Renaut Mosdale and Supramaniam Srinivasan, *J. Electrochimica Acta,* **40,** 413 (1995).
3. D. M. Bernardi and M. W. Verbrugge, *J. Electrochem. Soc.*, **139**, 2477 (1992).
4. M. L. Perry, J. Newman and E.J. Cairns, *J. Electrochem. Soc.*, **145**, 5 (1998).

5. T. V. Nguyen, *J. Electrochem. Soc.*, **143**, L105 (1996).

6. T. F. Fuller and J. Newman, *J. Electrochem. Soc.*, **140**, 1218 (1993).

7. T. V. Nguyen and R. E. White, *J. Electrochem. Soc.*, **140**, 2178 (1993).

8. A. C. West and T.F. Fuller, *J. Applied Electrochemistry*, **26**, 57 (1996).

9. V. Gurau, H. Liu and S. Kakac, *AIChE Journal*, **44**, 2410 (1998).

10. D. Singh, D. M. Lu and N. Djilali, *Int. J. Eng. Sci.,* **37**, 431 (1999).

11. S. Dutta, S. Shimpalee and J. W. Van Zee, *J. Applied Electrochemistry*, **30**, 135 (2000).

12. S. Shimpalee and S. Dutta, *J. Numerical Heat Transfer,* Part A, **38,** 111 (2000).

13. D. Natarajan and T. V. Nguyen, *J. Electrochem. Soc.*, **148**, 1324 (2001).

14. S. Um, C. Y. Wang and K. S. Chen *J. Electrochem. Soc.*, **147**, 4485 (2000)

15. J. S. Yi and T. V. Nguyen, *J. Electrochem. Soc.*, **146**, 38 (1999).

16. J. S. Yi and T. V. Nguyen, " A Two-Phase Flow Model to Investigate the Hydrodynamics of Gas and Liquid water in the Cathode of PEM Fuel Cells with Interdigitated Gas Distributors," Paper 107b, *AIChE Meeting*, Miami Beach, FL Nov.15-20, 1998.

17. W. He, J. S. Yi and T. V. Nguyen, *AIChE Journal*, **46**, 2053 (2000).

18. C. Y. Wang and P. Cheng, *Int. J. Heat Mass Transfer*, **39**, 3619 (1996).

19. R. B. Bird, W. E. Stewart and E. N. Lightfoot, *Transport Phenomena*, John Wiley & Sons, New York (1960).

20. L. A. Richards, *J. Physics,* **1**, 318 (1931).

21. J. Bear and Y. Bachmat, *Introduction to Modeling of Transport Phenomena in Porous Media*, Kluwer Academic Publishers (1991).

22. D. L. Wood (III), J. S. Yi and T. V. Nguyen, *Electrochim. Acta*, **43**, 3795 (1998)

23. Paik Woon-kie, T. E. Springer and S. Srinivasan, *J. Electrochem. Soc.*, **136**, 644 (1989).

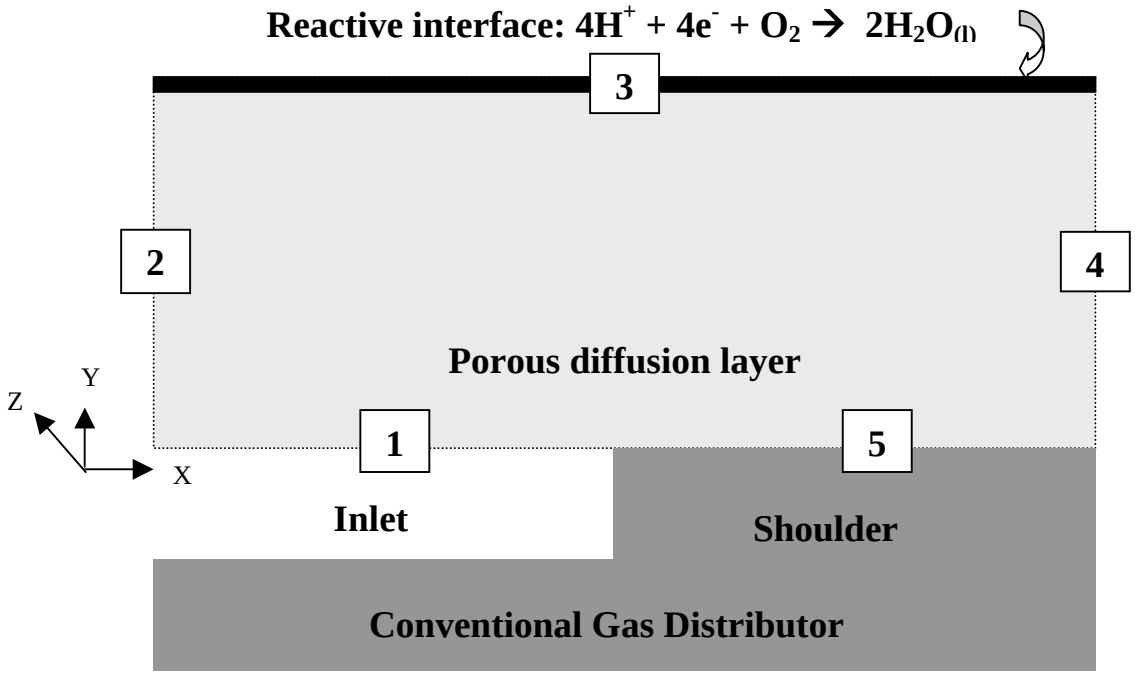


**Figure 1.** Cross section of model domains for conventional gas distributors.

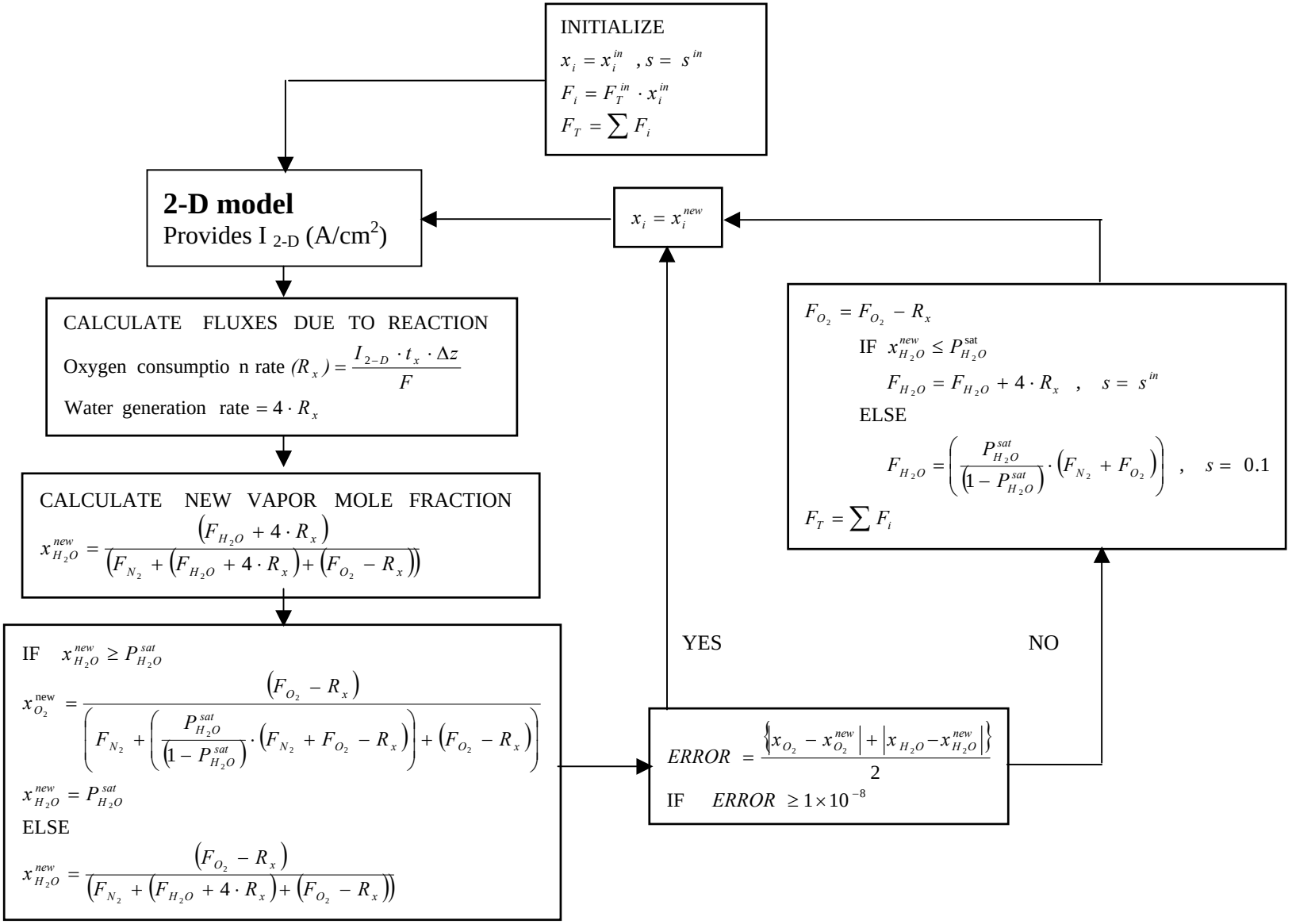


**Figure 2.** Schematic of solution procedure for 3-D model.

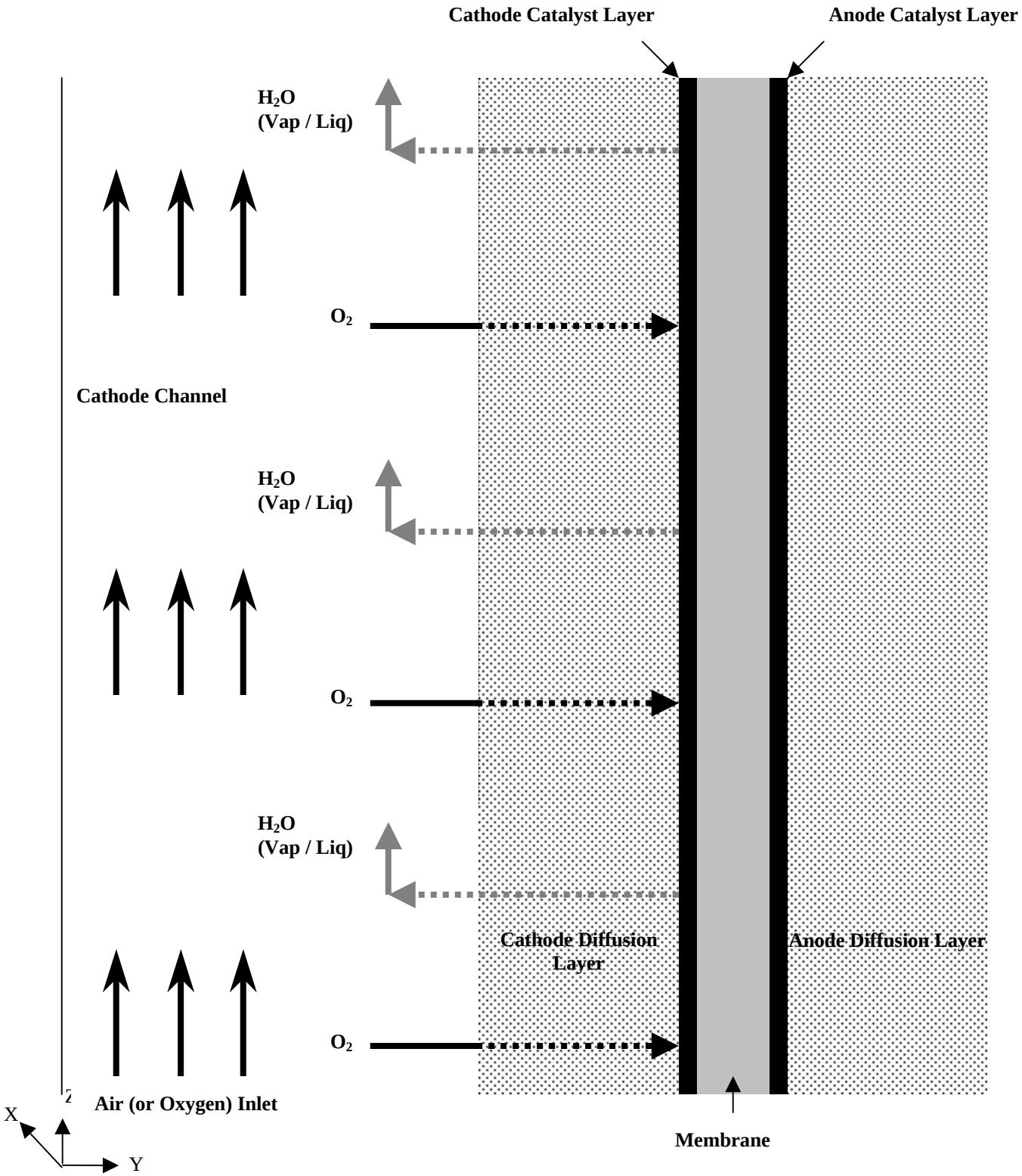


**Figure 3**: A schematic of the cathode chamber of PEM fuel cell using conventional flow distributors --- *Dashed line*: Slow diffusion (gas) / capillary (liquid) transport mechanism, *Solid line*: Fast convective flow (gas) / drag (liquid) mechanism

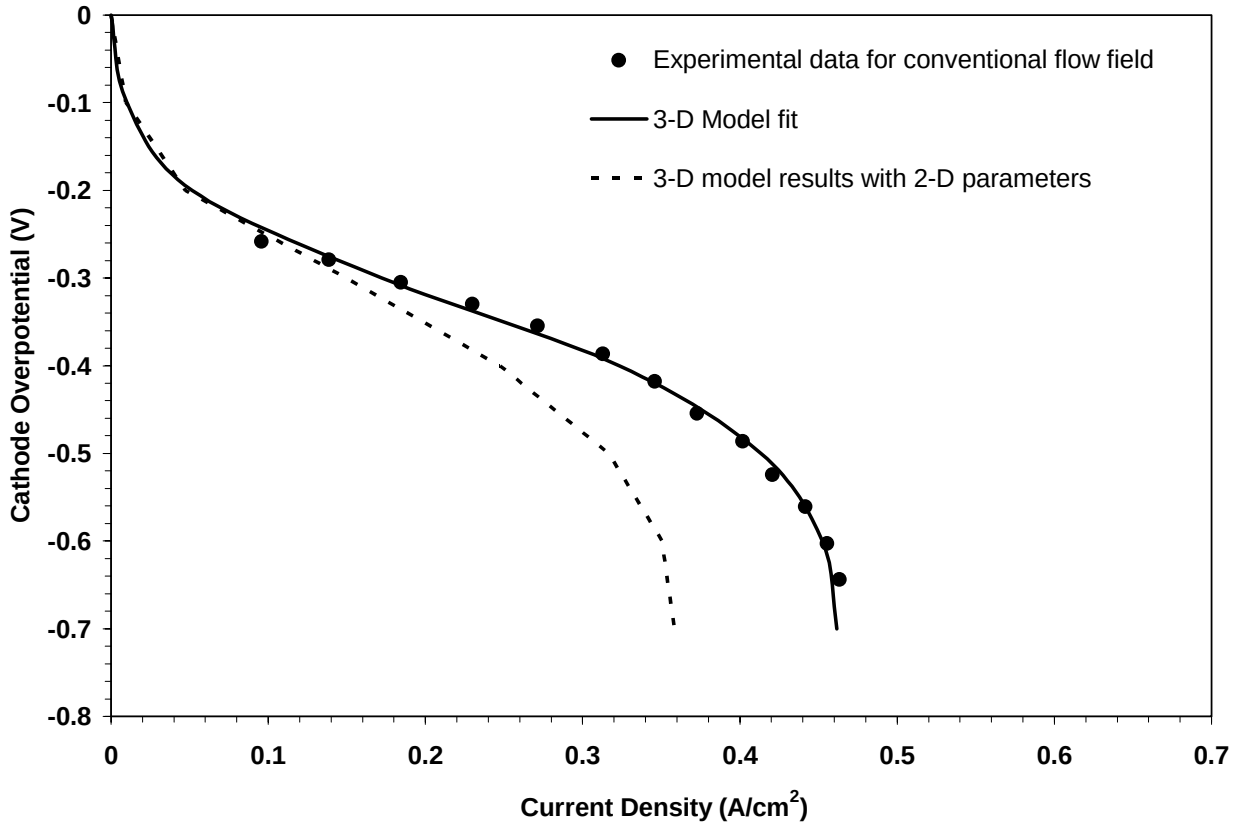


**Figure 4.** Comparison of model simulations to experimental data

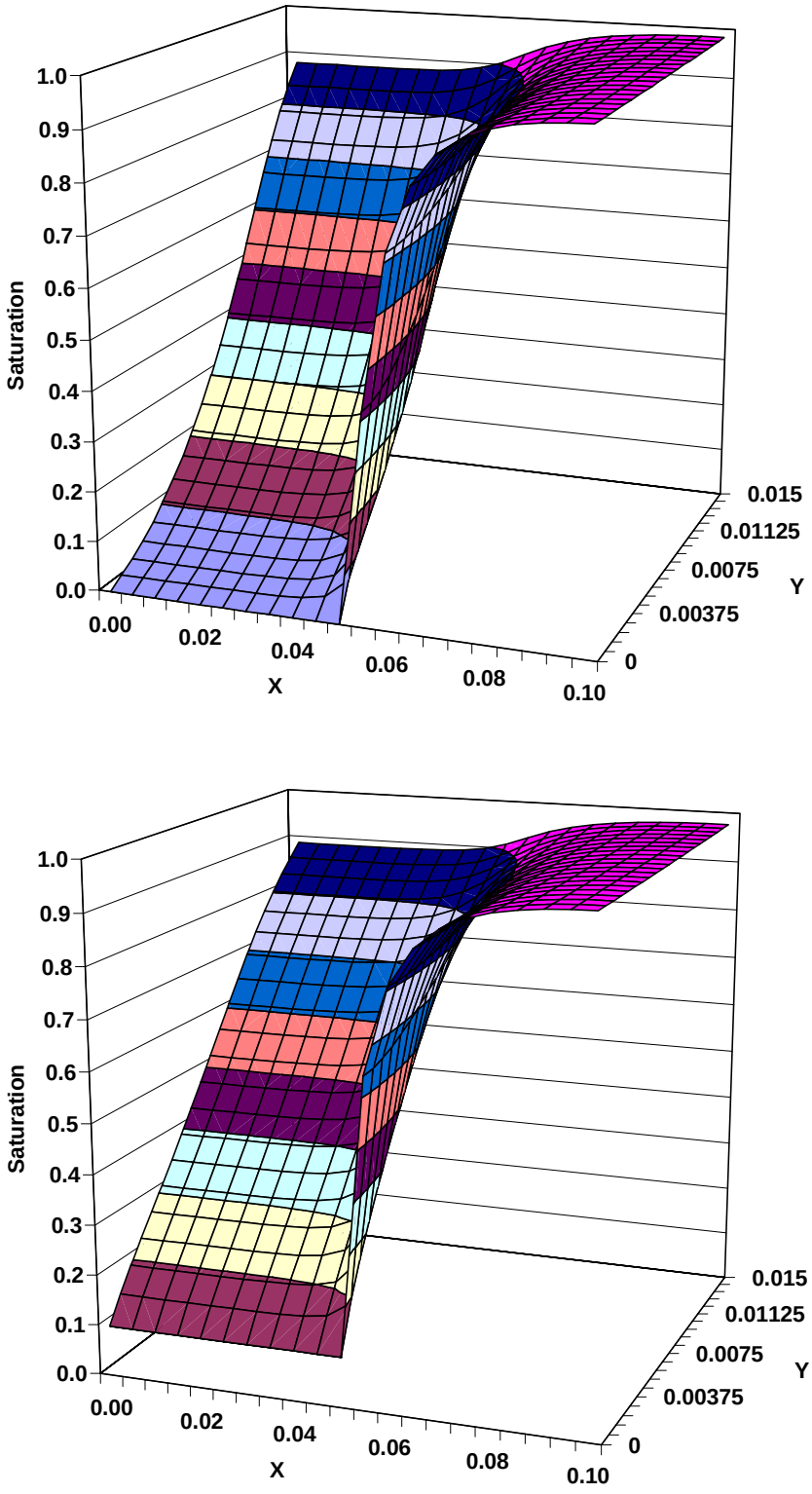


**Figure 5.** Liquid water distribution at the inlet (a) and exit (b) of conventional gas distributor.

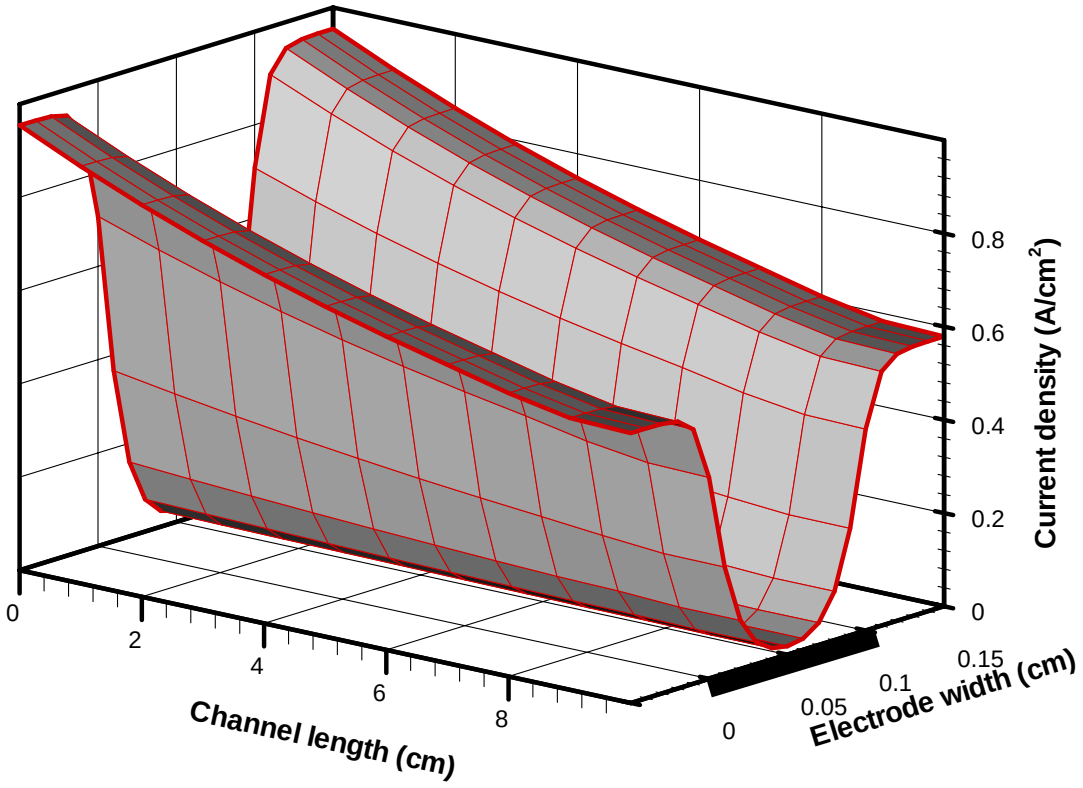


**Figure 6.** Current distribution along the length of the channel and electrode width.

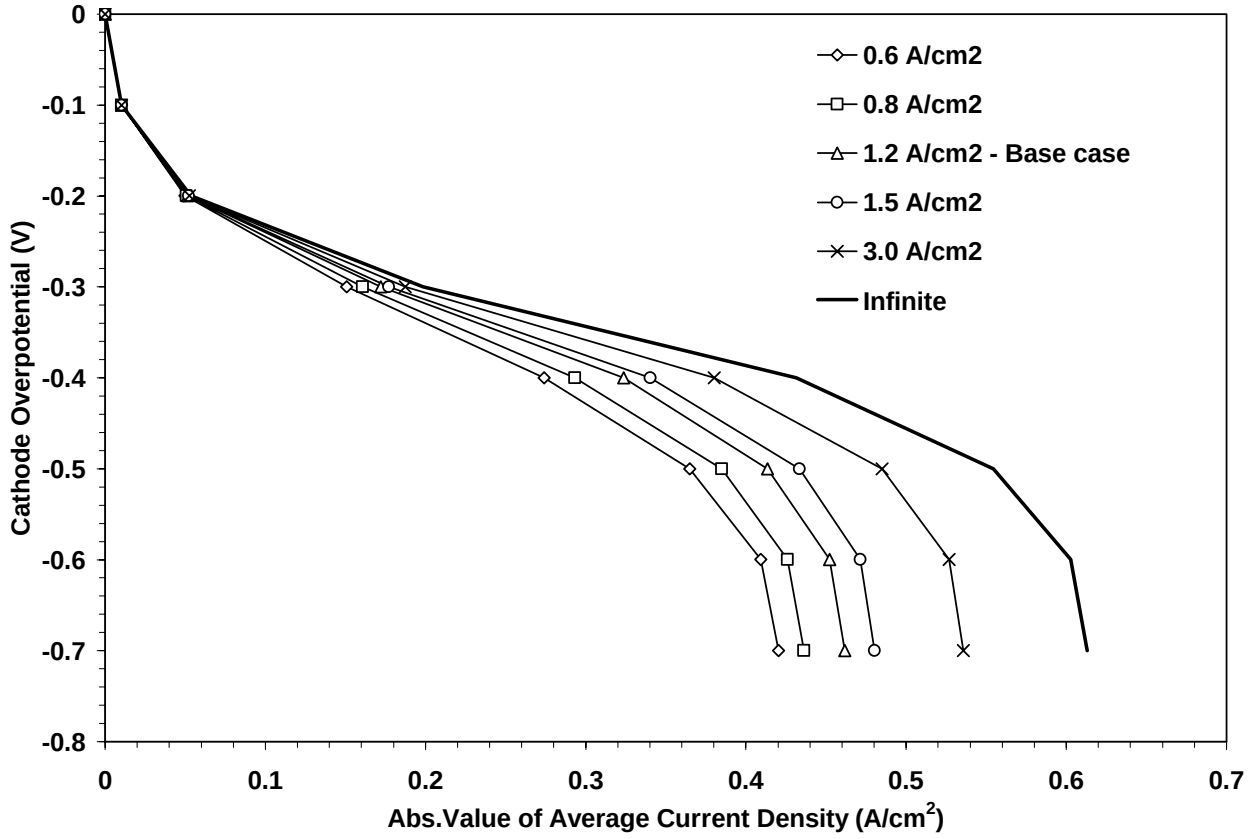


**Figure 7.** Effect of stoichiometric flow rate on cathode performance.

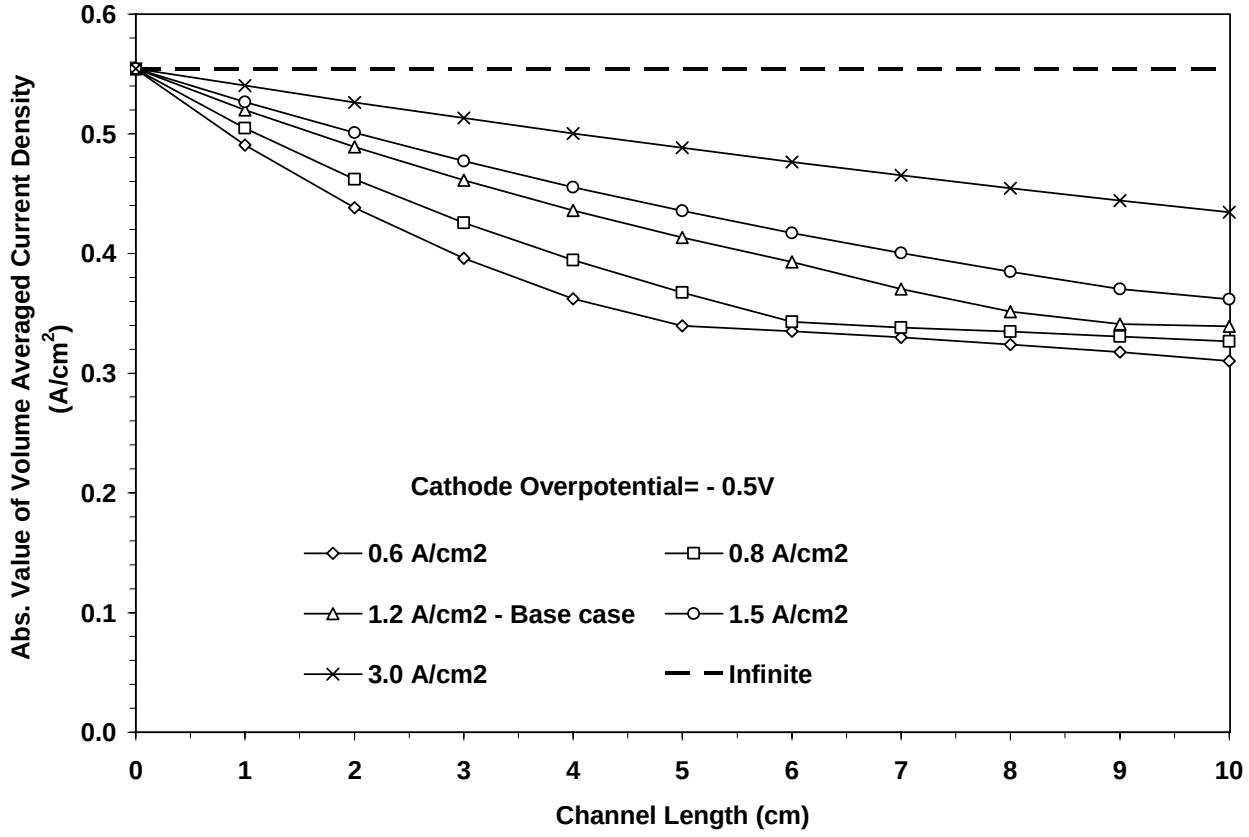


**Figure 8.** Current density variation along the length of the channel in a conventional flow distributor at different stoichiometric flow rates.

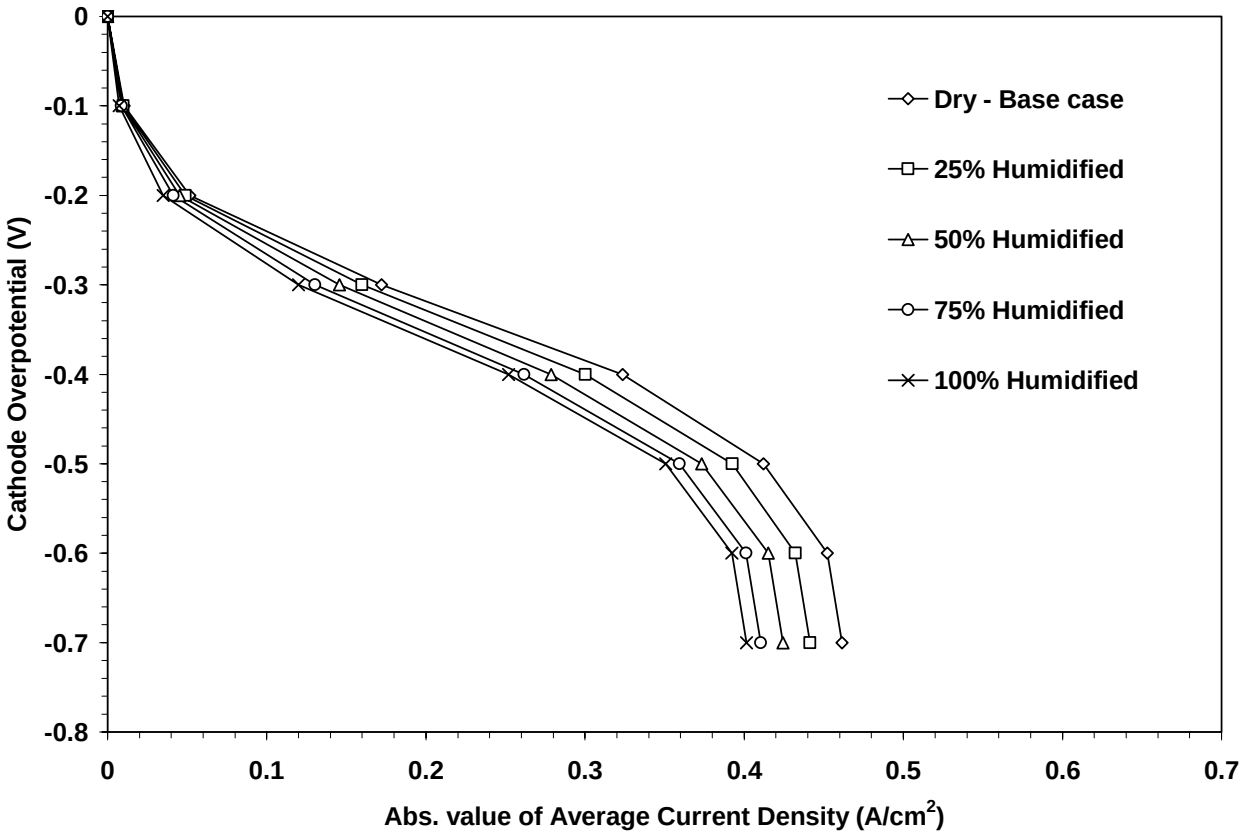


**Figure 9.** Effect of inlet stream humidity on cathode performance.

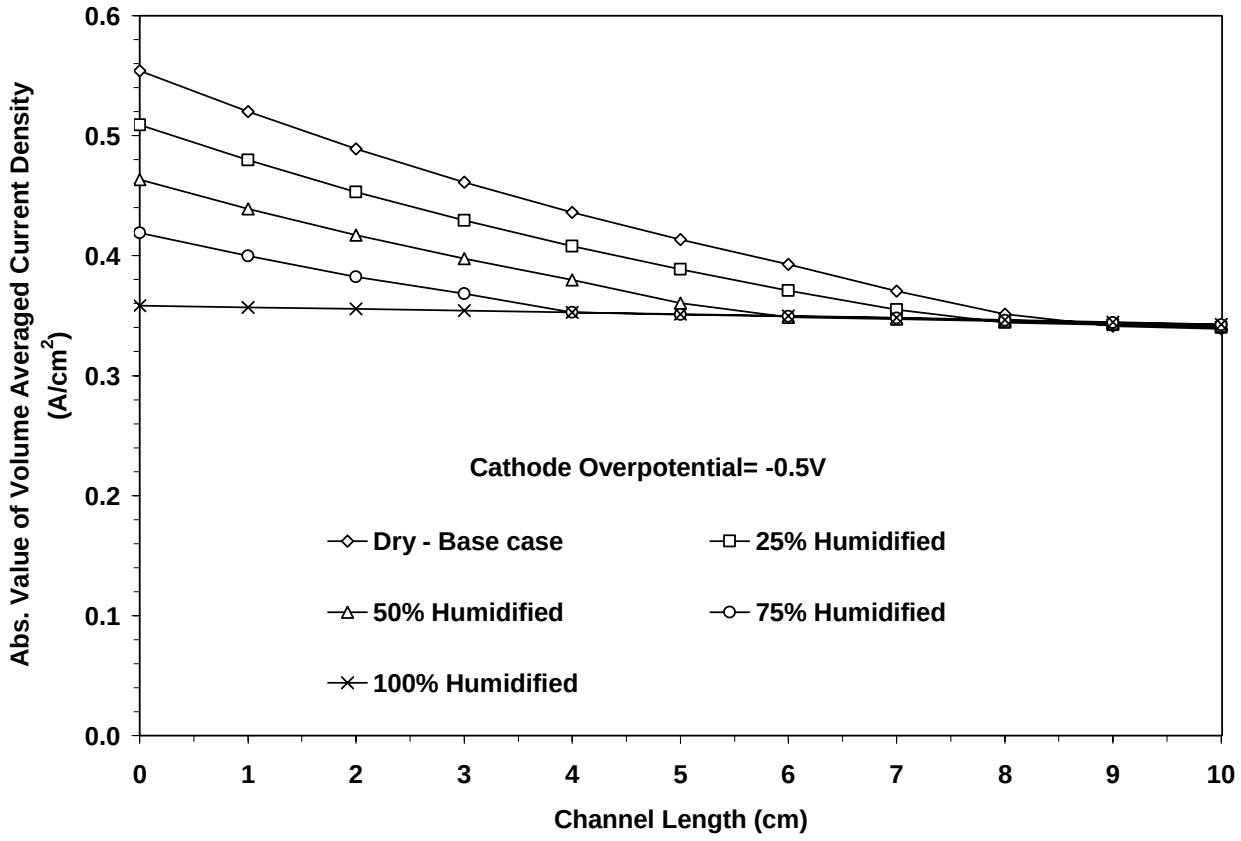


**Figure 10.** Current density variation along the length of the channel in a conventional flow distributor at inlet stream relative humidity.

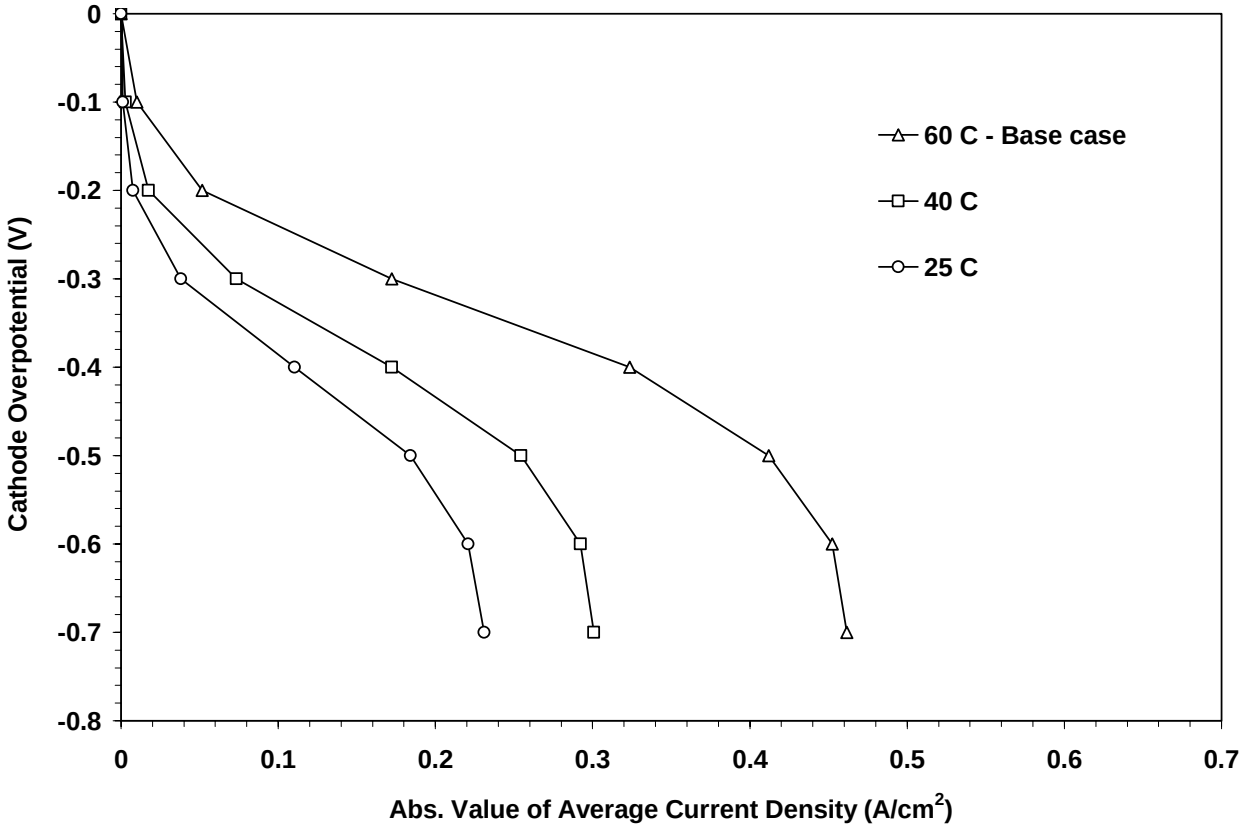


**Figure 11.** Effect of operating temperature on cathode performance.

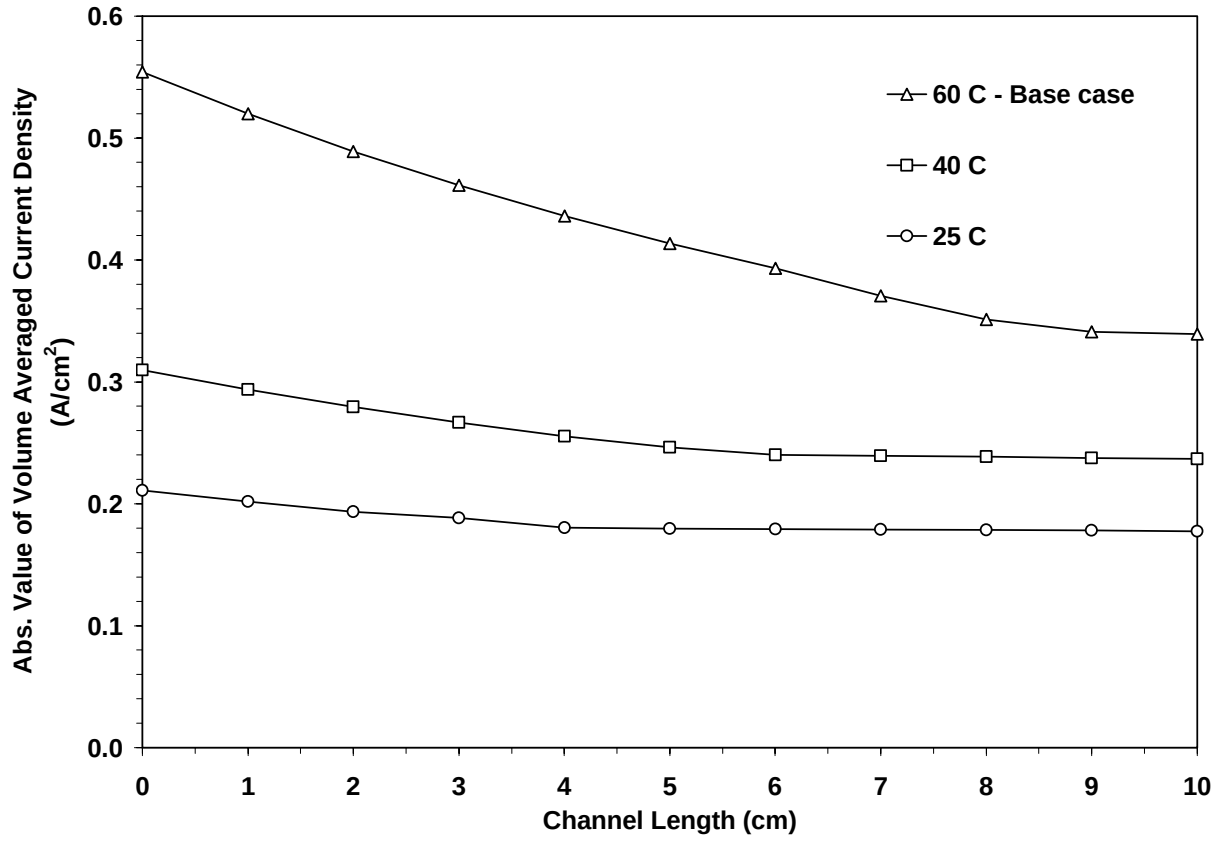


**Figure 12.** Current density variation along the length of the channel in a conventional flow distributor at various operating temperatures.

**Table 1.** Summary of governing equations and boundary conditions used in Natarajan et al's [13] work

**Governing equations within the diffusion layer**

Gaseous species

*Mass balance:* $\frac{\partial\left[\varepsilon_0(1-s)C_T x_i\right]}{\partial t}+\nabla\cdot N_i = R_i$ *Flux expression:* $\nabla x_i = \sum_{j=1}^{n}\frac{1}{C_T D_{ij}^e}\left(x_i N_j - x_j N_i\right)$

*where,* $R_{O_2}=0,$ $R_{H_2O}=\left(k_e\varepsilon_0\,\rho_w/m_w\, s\left(p_{H_2O}^{sat}-Px_{H_2O}\right)\right)\cdot switch-\left(k_c\varepsilon_0(1-s)x_{H_2O}\left(Px_{H_2O}-p_{H_2O}^{sat}\right)\right)\cdot(1-switch)$

$$switch=\left[\frac{1}{2}+\frac{1}{2}\frac{\left|p_{H_2O}^{sat}-Px_{H_2O}\right|}{\left(p_{H_2O}^{sat}-Px_{H_2O}\right)}\right]$$

Liquid water

*Mass balance:* $\varepsilon_0\frac{\partial s}{\partial t}+\nabla\cdot q_w=\frac{-m_w\cdot R_{H_2O}}{\rho_w}$ *Flux expression:* $q_w=\frac{-K(s)}{\mu}\left(\rho_w g\nabla\psi\right)=\frac{-K(s)}{\mu}\left(\rho_w g\left(-\frac{\partial\psi}{\partial s}\right)\nabla s\right)$

*where,* $\psi=\left\{\left[e^{[-A(s-C)]}-e^{[A(s-C)]}\right]+\mathrm{B}\right\}\times\mathrm{D}$ $\frac{\partial\psi}{\partial s}=-A\times D\times\left[e^{[-A(s-C)]}+e^{[A(s-C)]}\right],$ $K(s)=K_{l,abs}k_{l,rel}=K_{l,abs}(s+0.01)$

**Boundary conditions (see Figure 1)**

| | |
|---|---|
| Interface 1 | $x_{O_2}=x_{O_2}^{in},\quad x_{H_2O}=x_{H_2O}^{in},\quad s=0$ |
| Interface 2 & 4 | $\frac{\partial x_{O_2}}{\partial \mathrm{x}}=0,\quad \frac{\partial x_{H_2O}}{\partial \mathrm{x}}=0,\quad \frac{\partial s}{\partial \mathrm{x}}=0$ |
| Interface 3 | $N_{H_2O}=0,\quad N_{O_2}=\frac{-0.5I}{2F},\quad q_w=\left(\frac{m_w}{\rho_w}\right)\left(\frac{1}{2}+\alpha\right)\frac{I}{F},\quad I=I_0 a_0\left(2^{\left(\frac{T-273}{10}\right)}\right)(1-s)\frac{x_{O_2}P}{P_{ref}}\exp\left(\frac{-\alpha_c F\eta}{RT}\right)$ |
| Interface 5 | $\frac{\partial x_{O_2}}{\partial \mathrm{y}}=0,\quad \frac{\partial x_{H_2O}}{\partial \mathrm{y}}=0,\quad \frac{\partial s}{\partial \mathrm{y}}=0$ |

**Table 2.** Base case parameters used in the pseudo three dimensional model.

| | |
|---|---|
| Channel length | 10 cm |
| length of control volume | 1.0 cm |
| Exchange current density @ 273°K [a, 23] | 1.371 E-4 Amps/$cm^2$ |
| Liquid water permeability at 100% saturation | 1.5 x $10^{-10}$ $cm^2$ |
| Constants used in capillary head expression [13] (A,B,C and D (cm)) | 3.82, 21, 0.69 and 0.0133, respectively |
| Stoichiometric flow rate of air | 1.2 A/$cm^2$ |

[a] Obtained from reference 23 and adjusted for temperature and active surface area

See reference 13 for other relevant details on base case conditions